Heliyon 9 (2023) e14668

Contents lists available at ScienceDirect

Heliyon

journal homepage: www.cell.com/heliyon

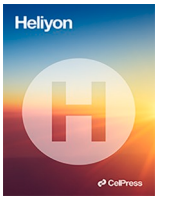

Research article

One-pot green synthesis of gold nanoparticles using *Sarcophyton crassocaule*, a marine soft coral: Assessing biological potentialities of antibacterial, antioxidant, anti-diabetic and catalytic degradation of toxic organic pollutants

Samson Rokkarukala [a], Tijo Cherian [a,**], Chinnasamy Ragavendran [b], Raju Mohanraju [a], Chinnaperumal Kamaraj [c], Yosif Almoshari [d], Ahmed Albariqi [d], Muhammad H. Sultan [d], Abdullah Alsalhi [d], Syam Mohan [e,f,g,*]

[a] *Department of Ocean Studies and Marine Biology, Pondicherry University, Port Blair campus, Brookshabad, Port Blair, Andamans- 744112*
[b] *Department of Conservative Dentistry and Endodontics, Saveetha Dental College and Hospitals, Saveetha Institute of Medical and Technical Sciences (SIMATS), Chennai, India*
[c] *Interdisciplinary Institute of Indian System of Medicine (IIISM), Drug Testing Laboratory, Directorate of Research, SRM Institute Science and Technology, Kattankulathur - 603 203, Tamil Nadu, India*
[d] *Department of pharmaceutics, College of pharmacy, Jazan University,P.O. Box 114, Jazan 45142, Saudi Arabia*
[e] *Substance Abuse and Toxicology Research Centre, Jazan University, Jazan, Saudi Arabia*
[f] *School of Health Sciences, University of Petroleum and Energy Studies, Dehradun, Uttarakhand, India*
[g] *Center for Transdisciplinary Research, Department of Pharmacology, Saveetha Dental College, Saveetha Institute of Medical and Technical science, Saveetha University, Chennai, India*

A R T I C L E I N F O

Keywords:
Sarcophyton crassocaule
Soft coral
Gold nanoparticles
Antibacterial
Antioxidant
Antidiabetic
Catalytic activity
Organic pollutants

A B S T R A C T

Marine bio-resources are being extensively researched as a priceless supply of substances with therapeutic potential. This work report the first time attempt made towards the green synthesis of gold nanoparticles (AuNPs) using the aqueous extract of marine soft coral (SCE), *Sarcophyton crassocaule*. The synthesis was conducted under optimized conditions and the visual coloration of reaction mixture changed from yellowish to ruby red at 540 nm. The electron microscopic (TEM, SEM) studies exhibited spherical and oval shaped SCE-AuNPs in the size ranges of 5–50 nm. The organic compounds present in SCE were primarily responsible for the biological reduction of gold ions validated by FT-IR while the zeta potential confirmed the overall stability of SCE-AuNPs. The synthesized SCE-AuNPs exhibited variety of biological efficacies like antibacterial, antioxidant and anti-diabetic in nature. The biosynthesized SCE-AuNPs demonstrated remarkable bactericidal efficacy against clinically significant bacterial pathogens with inhibition zones of mm. Additionally, SCE-AuNPs exhibited greater antioxidant capacity in terms of DPPH: 85 ± 0.32% and RP: 82 ± 0.41%). The ability of enzyme inhibition assays to inhibit α-amylase (68 ± 0.21%) and α-glucosidase (79 ± 0.2%) was quite high. The study also highlighted the spectroscopic analysis of the biosynthesized SCE-AuNPs' catalytic effectiveness of 91% in the reduction processes of the perilous organic dyes, exhibiting pseudo-first order kinetics.

** Corresponding author.
* Corresponding author. .
E-mail addresses: tvarghese891@gmail.com (T. Cherian), syammohanm@yahoo.com (S. Mohan).

https://doi.org/10.1016/j.heliyon.2023.e14668
Received 28 January 2023; Received in revised form 8 March 2023; Accepted 15 March 2023

1. Introduction

With the development of innovative materials that differ from their bulk equivalents in terms of their properties, nanotechnology has enabled significant scientific advancements and transcending boundaries of applications arraying from physics and engineering to biomedical and pharmaco-kinetics [1–4]. The integration of green chemistry principles to nanotechnology with a strict emphasis on structural modalities (shape, size and surface morphology) employs a vital role in supervising and moderating the optical, physico-chemical, and electronic properties of nanomaterials, thus, accentuating a key subject of concern in nanoscience research. Nano-particles are solid lattice structures, of size <100 nm in general, with profound applications in catalysis, optoelectronics, sensing and drug delivery, intersecting contours of diverse scientific domains [5,6].

Among various nano-sized particles, gold nanoparticles (AuNPs) have attracted a merited thoughtful consideration owing to its fine tunable properties of size, shape, surface area to volume ratio and plasmon resonance [7]. Its efficient applications in the field of drug and tissue delivery, tumor imaging, photothermal and cancer therapy, immune-chromatographic based identification of pathogens and gene therapy has acknowledged it as the "magic bullets" for biomedical crafts and technologies. Apart from its structural artifact, the accreditations of safety, biocompatibility and targeted delivery, confers it as "best suitable candidates" of therapeutic vectors [7,8].

Over the past years, many synthetic procedures pertaining to metal nanoparticles synthesis have been carried out by orthodox physical and chemical methods. Despite high yield and specificity of size and shape of generated nanomaterials, the constraints of costly and expensive production and processing technologies, involvement of hazardous chemical substances and high thorough put of energy, greatly limits their relevance in biomedical applications [9]. Underscoring the aforementioned concerns, research has shifted towards the dynamic and incredibly diverse biological entities for synthetic strategies, paving a "green route" of biocompatibility, low economics and eco-safeness [10]. The phytogenic process of nano-synthesis is generally employed, due to its economical and relatively simpler in application, often generating polydispersednanoparticles, pertaining to diverse photochemistry of plant parts and types [6, 11]. In contrast, the microbial mediated synthesis has gained vast contemplation in recent times, as microorganisms are "prospective bio-factories" for the green synthesis of nanomaterials, reflecting their technological and indispensable importance. Microbial derived nanoparticles of diverse sizes and shapes have been reported in various species of bacteria, fungi and yeasts but limit their large scale applicability due to the maintenance of aseptic cultural conditions and pure cell cultures [12]. Previous researches showed that terrestrial plants have been widely studied used to make metal nanoparticles, and very sparse reports pertain to the synthesis of nanogold off of marine resources that are renewable, easy available and environmentally facile. In recent times, marine macroalgae has emerged as the prospective source of nanogeneration as it is rich in bioactive compounds with applicative insights in both biotechnology and industrial domains.

The microbial infections are becoming increasingly resistant to numerous drugs over time. Antibiotics are no longer effective at preventing or treating infectious diseases. There is an urgent need to find new, alternative antimicrobial medications with distinct modes of action to combat resistant microorganisms [2]. Treatment of other chronic diseases like diabetes and cancer is also impacted, and infectious infections become more challenging to cure [3].It is a monumental endeavor to overcome drug resistance that microorganisms have acquired as it can be executed through a variety of mechanisms [10].As a solution, nanotechnology has emerged to alter the current situation and halt the spread of drug resistance. The drug conjugated nanoparticles, a brand-new clinical tool, can help in combating antibiotic resistance by enhancing the inhibitory effects of antibiotics, making them a vitally important and effective therapeutic alternative for the treatment of infection-related drug resistance [6,7]. As a result, nanoparticles are viewed as the next generation of antibiotics.Also, the primary factor resulting in tissue damage, oxidative stress, is linked to a wide range of chronic diseases, including cancer, heart disease, diabetes, liver disorders, and neurological disorders [7]. An imbalance between free radicals and the antioxidant defence mechanism, which results in oxidative stress, leads to poor health, health issues and difficulties, diseases, and disorders. Oxidative stress arises when the production of free radicals exceeds the cellular antioxidant levels. Another cause of oxidative stress is the fact that cells can occasionally produce less antioxidants, which elevates the level of ROS/antioxidant ratio [10]. With the development of nanotechnology, prime focus has shifted to green metal nanoparticles for usage as antioxidants. Because green manufactured nanoparticles, with their distinctive properties and varied surface characteristics, display synergistic effect, their effectiveness has surpassed that of their bulk counterparts [7].Further, the enzymes called α-glucosidase and α-amylase, which are secreted in the small intestine, are necessary for carbohydrate metabolism as they hydrolyze glycoside bonds from complex carbohydrates at various locations to form α-glucose [11[. These unchecked activities of these enzymes raise postprandial glucose, which causes an imbalance between insulin secretion for glucose uptake and systemic glucose absorption. In the management of Type-2 diabetes (T2D), it has been observed that inhibiting the activity of the enzymes α-glucosidase and α-amylase lowers the risk of obesity, renal failure, and cardiovascular illnesses [12].Traditional anti-diabetic medications likeacarbose, voglibose, miglitol, and metfomin are frequently administered to prevent hepatic cells from producing glucose as a result of the breakdown of carbohydrates by α-glucosidase and α-amylase enzymes [11]. Nonetheless, there is a need for the investigation of substitute medications in the nano range due to the probable negative effects of increased gas buildup in the intestine and liver toxicity on prolonged use. As a result, medications derived from natural sources are required.Due to its extensive surface area, biocompatibility, and simplicity of biomolecular functionalization for active drug delivery, gold nanoparticles, are being used increasingly in biomedicine and therapeutics [13]. This characteristic of gold nanoparticles may aid in preventing the potential removal of medications from the systemic circulation by the functions of spleen and liver. Diverse industrial activities dump a variety of water contaminants and dyes into water bodies, with a medial concentration of 10–200 mg per litre (mg/l) [13]. They are classified contaminants with adverse effects due to non-biodegradability, carcinogenicity, and mutagenicity with grave implications on both human and aquatic health [14]. Additionally, it causes a host of medical conditions such liver disease, renal damage, skin cancer, and the toxicity of both human and animal

central nervous systems [7]. In case of living beings, 4-Nitrophenol is known for its genotoxicity and carcinogenicity nature, and its transformation is limited by its strong stability and low aqueous solubility [15]. In addition, synthetic dyes like bromophenol blue and methyl red are widely utilized in culinary, cosmetic, pharmaceutical, textile, leather, and dyeing sectors. Since 30–40% of these dyes occur in the aqueous phase and adds visual coloration to the effluent waste without causing unalluring pollution or eutrophication, they are regarded as the most troublesome chemicals. Additionally, these dyes are also carcinogenic, mutagenic, poisonous, and non-biodegradable in nature, causing the creation of hazardous by-products in water bodies [16]. Although, there are several techniques for removing these contaminants including ion exchange adsorption, chemical precipitation and filtration, they are not very effective. It is therefore highly desirable to eliminate these harmful contaminants by utilizing effective and risk-free methods.

Natural chemical defenses are employed by marine species, particularly those that are fixed or slowly moving, to defend them against harmful predators, challenging environmental conditions, and/or the encroachment of rivals. Natural products from marine animals are increasingly being recognized as a key source of new medicines because of the biological and chemical richness of marine habitats, as well as the discovery and improved knowledge of marine secondary metabolites with distinctive chemical structures and biological activities [17]. Soft corals are primarily rich potential source of pharmacological leads among marine invertebrates. Numerous species of soft corals have produced a plethora of distinctive secondary metabolites, including sesquiterpenoids, diterpenoids, steroids, and other chemical substances [18–20]. Importantly, it has been shown that several of the natural substances derived from soft corals exhibit a range of biological actions, including anti-tumor, antiviral, antifouling, and anti-inflammatory effects [17, 21].

Hence, the destined attempts on marine resources for the exploration of secondary metabolites have evoked a tempting surveillance for the biological production of metallic nano-colloids. In light of this and taking into account the biological diversity of marine organisms, we investigated and produced stable gold nanoparticles by reducing aqueous chloroauric acid with an aqueous extract of marine soft coral, *Sarcophyton crassocaule*. It's interesting to note that this is the first publication on the manufacture of stable gold nanoparticles utilizing marine soft coral.

2. Results and discussion

The literature survey has revealed the capability of vast sum of biotic species like marine bacteria {*Citricoccus* [5]; *Lysinibacillus odysseyi* [7];*Marinobacter pelagius* [22]}, fungi {*Fusarium oxysporum* and *Aureobasidium pullulans* [23]}, algae {*Turbinaria conoides* [24] and *Sargassum crassifolium* [25]} in synthesizing the gold colloidal nanoparticles. Here, it is the first report of AuNPs biosynthesis by using marine soft coral *S. crassocaule*.

The optical properties of metal nanoparticles are primarily studied by UV–visible spectroscopy to ascertain the formation and stability of synthesized nanoparticles in the aqueous solution. The initial confirmation of SCE-AuNP formation was the change in colour of the reaction medium from pale yellowish to dark violet, after 30 min following the addition of extract, which is mainly attributed to the excitation of surface plasmon vibrations. The production of gold nanoparticles was clearly indicated by a band in the UV–visible spectrum found at 540 nm corresponding to the surface plasmon resonance (Fig. 1a). The positional and spatial changes in absorbance peaks mostly depends on particle size, concentration of metal solution, ligands or reducing agents, type and amount of extract and dielectric constant of the medium, etc [7]. Additionally, the electromagnetic field-induced collective oscillation of free electrons in metallic nanoparticles, known as the SPR effect, is primarily responsible for the change in colour of the reaction mixture [4,14]. The change in colour is an indicative of simultaneous change in the oxidation states of metal ions. Similar results were also observed at absorbance values of 520–550 nm as reported by the studies of [7,14,26–29]. Further, no change in absorbance peaks was observed at time intervals (Day 1- Day 60) (Fig. 1b), thereby, suggesting the formation of stable SCE-AuNPs showing no aggregation.

The TEM images (Fig. 2a), particle size distribution histogram (Fig. 2b) and SAED pattern (Fig. 2c) displays well dispersed spherical

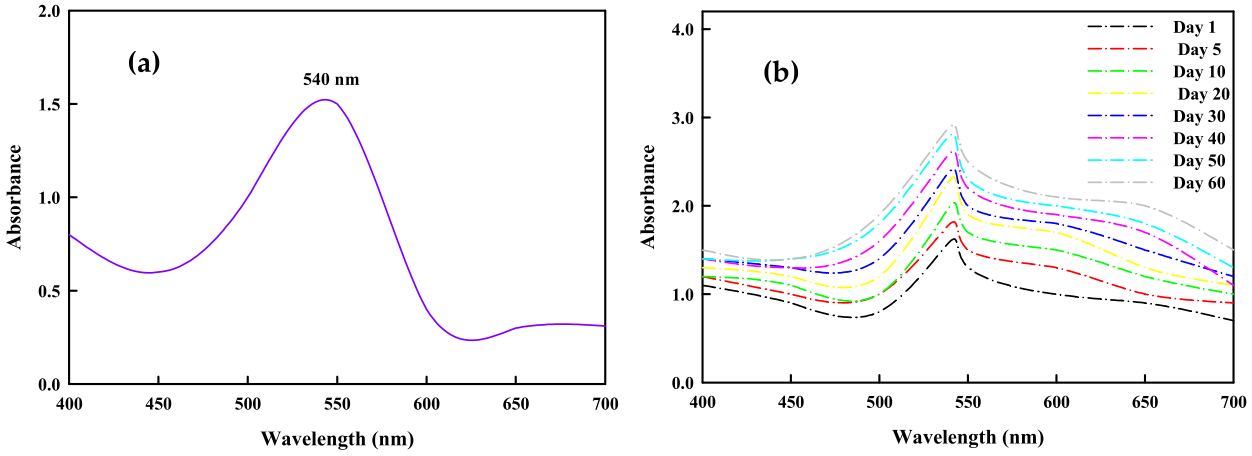

Fig. 1. Ultraviolet–visible (UV–vis) spectra of (a) SCE-AuNPs, (b) stability peaks recorded over time.

particles with regular distribution. The mean particle size of the synthesized SCE-AuNPs was found to be 30.83 nm. The observed particles were extremely mono-dispersed which could be due to the presence of some major organic biomolecules in the aqueous extract of soft coral, acting as a ligand which proficiently stabilizes, modulates and reduces synthesized SCE-AuNPs (from Au^{+} to Au^{0}) and thus limits and controls the growth and clustering of nanoparticles. The particle size histogram inferred the size ranges of SCE-AuNPs to be 5–50 nm. The SEM micrographs were found to be in well correlation with the TEM results (Fig. 2d). Similar report was also observed in *Lawsoniainermis*-AuNPs [14]; *Euphorbiahirta*-AuNPs [30]; *Leucosideasericea*-AuNPs [31]; *Acanthophoraspicifera*-AuNPs [32]. The stability of SCE-AuNPs was quantified by the measurements of zeta potential. The nanoparticles are sufficiently stabilized in solutions when their zeta potential is > 20 mV or < -20 mV [33]. The zeta potential value of SCE-AuNPs was found to be −22.129 mV indicating negative surface charges on the nanoparticles (Fig. 3a). The electrostatic repelling forces among nanoparticles are supported by the negative surface change, which enhances stability and prevents aggregation [34]. Additionally, negatively charged nanoparticles tend to provide better stability and avoid particle aggregation, leading to stable nanoparticles [35,36]. Therefore, it has been determinative with reference to the stability of nanoparticle dispersions by using the extent of repulsion and attraction quantified by zeta potential [37]. The measurements of negative zeta-potential of SCE-AuNPs were discovered to be within the typical range for stable nano-colloidal dispersions. Further, the investigations on the thermal behavior of the biosynthesized SCE-AuNPs were studied by TGA (Fig. 3b). The first weight loss was observed at temperature region 100–180 °C attributable to the evaporation of adsorbed water molecules of the capping extract SCE. Following, the second stage loss of weight was observed (300–500 °C) where the smoldering of organic entities have taken place [38].

The FTIR spectra of SCE and SCE-AuNPs exhibited different characteristic peaks (Fig. 4). The SCE sample showed the absorption peaks at 3452, 3349, 2342, 2102, 2097, 1628; 1113, 1091, 1200; and 1159 cm^{-1} assigned to the vibrations of –OH stretch, –CH and $–CH_2$ of aliphatic hydrocarbons, –C═O (carbonyl group), aromatic ring stretch and ethereal C–O asymmetric stretch from pyran-derived ring structure of condensed biological molecules, respectively [39,40]. The most pronounced absorption peak observed at 3452 cm^{-1} was designated to hydroxyl (-OH) stretch which may be responsible for the reduction of metal ions to metal nanoparticles. The emergence of prominent carbonyl peak and the diminution of the normal hydroxyl peak points to the oxidation of biochemical entities present in SCE [41].

Due to the fact that gold occurs in solution as $AuCl_4^-$, a very potent oxidising agent, it may be possible to reduce Au(III) to Au(0) through this process [24]. In the presence of $AuCl_4$, the phenolic and aromatic compounds underwent oxidation to converting their hydroxyl groups to carbonyl groups. In a Red/Ox system, these biological molecules can transfer their π-electrons of C═O (carbonyl

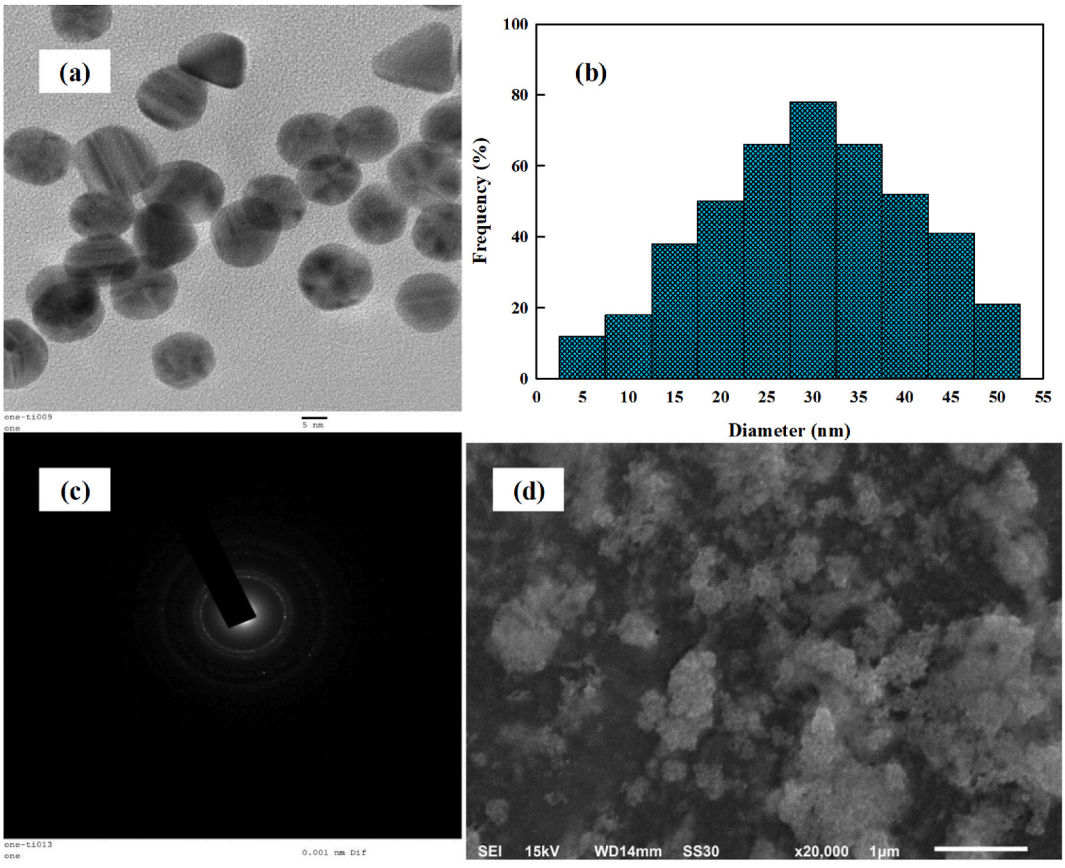

Fig. 2. Morphological analysis (a) TEM, (b) size distribution histogram, (c) SAED pattern, and (d) SEM of the biosynthesized SCE-AuNPs.

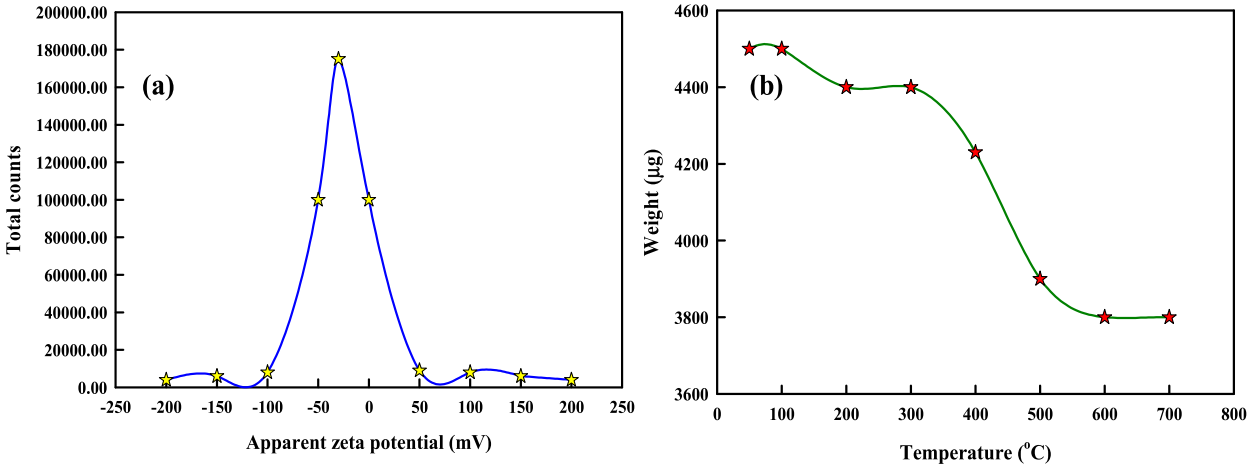

Fig. 3. Characterization of SCE-AuNPs. (a) Zeta potential, and (b) TGA.

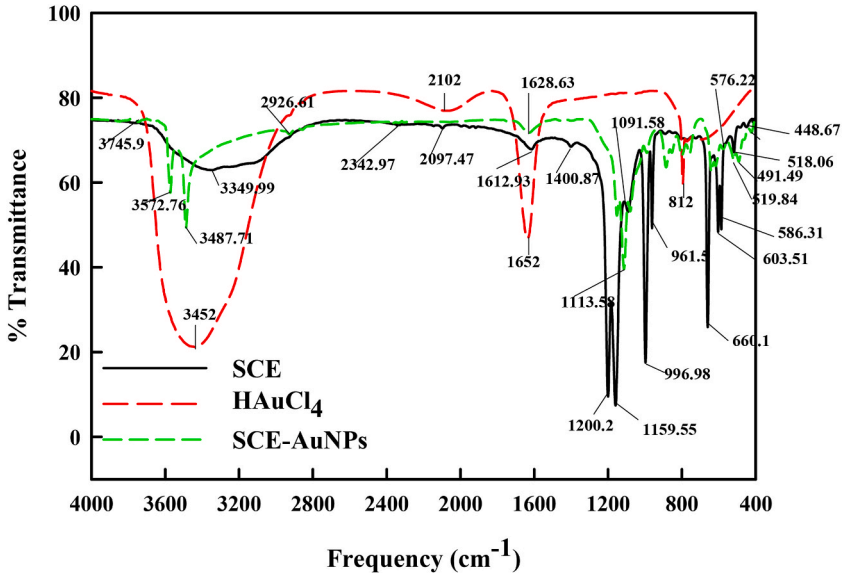

Fig. 4. FTIR spectra of $HAuCl_4$, SCE, SCE-AuNPs.

groups) to the free orbital of metal ions transforming them to metallic particles. The linkage bonding between C═O groups and metal ionic species furnishes unique signatures in the FT-IR peak spectra. The peak shift at 1628 cm^{-1} following the formation of gold nanoparticles is ascribed to the binding of the nanoparticles with the carbonyl groups. Additionally, the FT-IR analysis of SCE post synthesis of AuNPs revealed new peaks at 1113 and 1091 cm^{-1}, indicating formation of new bonds between the functional groups of organic molecules present in SCE and metallic nanoparticles. Therefore, it may be assumed that biological molecules such as phenols, flavonones and aromatic compounds operate as a capping agent in the fabrication of AuNPs and assists in stabilizing them under physiological settings [42,43].

The bioreduction of gold ions (Au^{3+}) to AuNPs (Au^0) through a biochemical-based process, in which the aqueous extract of soft coral consists reducing molecules including phenols, antioxidants, flavonones like compounds, aromatic and nitro-compounds, are included in the suggested mechanism underpinning the formation of AuNPs. The propensity of phenols and flavonones to give electrons or hydrogen atoms are well recognized [44]. Given that these biochemicals are powerful reducing agents, it is likely that they contribute in the bioreduction of $HAuCl_4$ to AuNPs through free electrons. According to one theory, gold clusters are created by first reducing gold ions (Au^{3+}) to "seed" particles (Au^0) [45]. These gold clusters are regarded as nucleation centres then aids in the reduction of any residual gold ions [14,46]. Using biochemicals found in the SCE, Fig. 5 describes the likely method for reducing gold salt (Au^{3+}) to AuNPs (Au^0).

The antioxidant activity of SCE and SCE-AuNPs, determined by DPPH and reducing power (RP) assays, was evaluated. The reaction mechanism of free radical scavenging process in the presence of biosynthesized SCE-AuNPs was analyzed by recording UV–visible

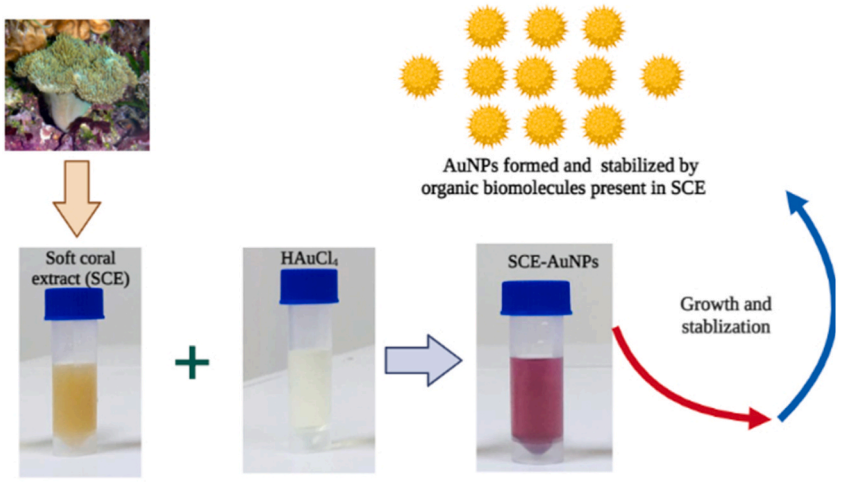

Fig. 5. Mechanism of AuNPs biosynthesis using soft coral extract (SCE).

spectra in range of 400–700 nm (Fig. 6). The maximum wavelength of DPPH· (kmax = 517 nm) of the compound gradually shifts from purple to pale yellow during the progression of the reaction. The findings indicate that the biofabricated SCE-AuNPstransform the DPPH· free radical to pale yellow colored stable DPPH-H by transferring an electron or hydrogen at atomic level [47]. Fig. 6a displays the effect of SCE-AuNPs on the activity of DPPH radical scavengers. The radical scavenging activity of DPPH increases together with the concentration of SCE-AuNPs. When compared to SCE, SCE-AuNPs exerted pronounced free radical scavenging activity (85 ± 0.32% and reducing power (82 ± 0.41%)(Fig. 6b), but was lower than the ascorbic acid standard (94%). The adsorption of biological molecules present in SCE on the biosynthesized spherical SCE-AuNPs with a greater surface area can be used as an explanation for the increased activity of SCE-AuNPs. Also, due to the large surface area to volume ratio, the free radical scavenging activity of different biological manufactured nanoparticles has also recently been reported [7,48,49].

Alpha(α)-amylase, an enzyme found in human saliva, can convert complicated starch molecules into simple glucose. Therefore, inhibiting α-amylase could regulate how carbohydrates are metabolised, which also reduces how much glucose is to be absorbed. In current investigation, the observed % inhibition of α-amylase by SCE and SCE-AuNPs is depicted in Fig. 7a. When compared to SCE, SCE tagged AuNPs displayed the strongest alpha amylase inhibitory activity, with 68 ± 0.21% inhibition. The positive control acarbose demonstrated strong α-amylase inhibitory action. According to earlier findings, the marine derived -biological molecules and -chemicals have the power to stifle the α-amylase enzyme [50,51]. Further, a key strategy for preventing a sharp rise in blood sugar is to inhibit the starch-blocking enzyme α-glucosidase. In the current investigation, SCE-AuNPs, SCE, and acarbose at various concentrations were investigated. The reaction diagram for the α-glucosidase inhibition caused by SCE-AuNPs is illustrated in Fig. 8. The obtained results demonstrated the % α-glucosidase enzyme inhibition was seen in ascending sequence (Fig. 7b). As expected, SCE-AuNPs exhibited promising inhibitory activity (79 ± 0.2%) than SCE, demonstrating its relative efficacy as a glucosidase inhibitor. The standard medication, acarbose which is classified as a potent inhibitor of α-glucosidase showed 86% inhibition. It is interesting to note that the % inhibition of SCE-AuNPs was found to be lower than that of acarbose, and this difference was statistically

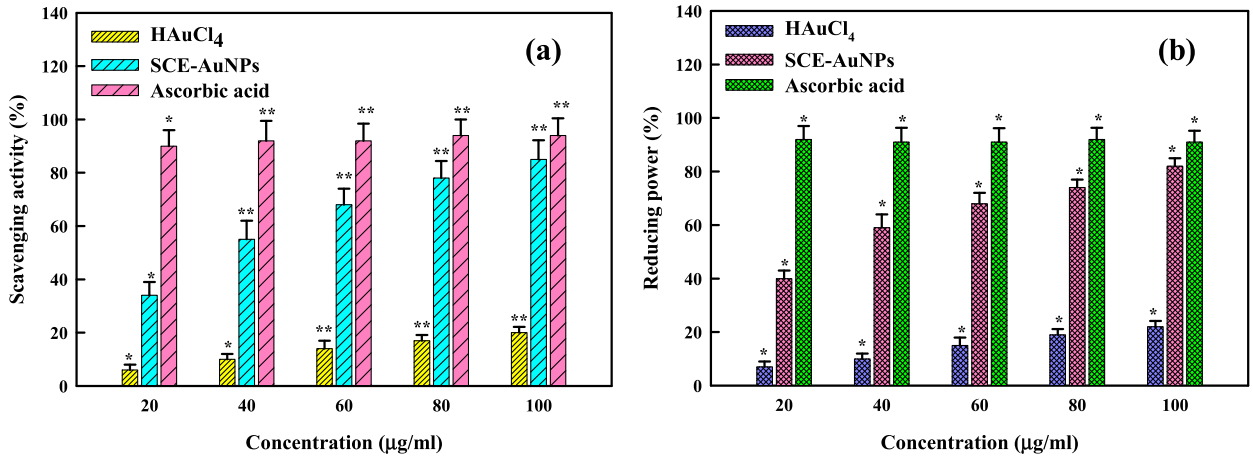

Fig. 6. In-vitro antioxidant activity of SCE-AuNPs (a) DPPH, and (b) Reducing power assay.

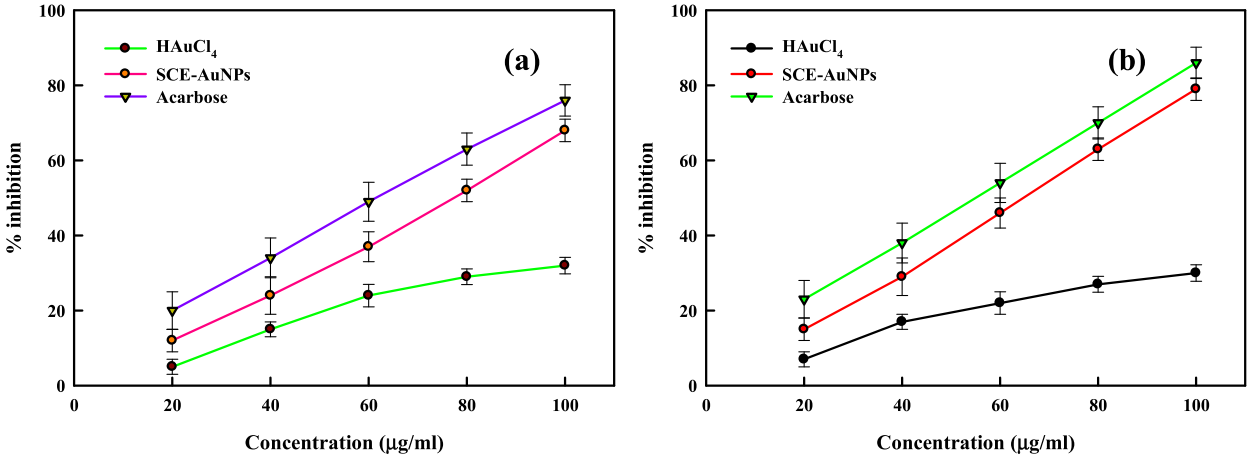

Fig. 7. In-vitro antidiabetic activity of SCE-AuNPs, (a) α-amylase and (b) α-glucosidase.

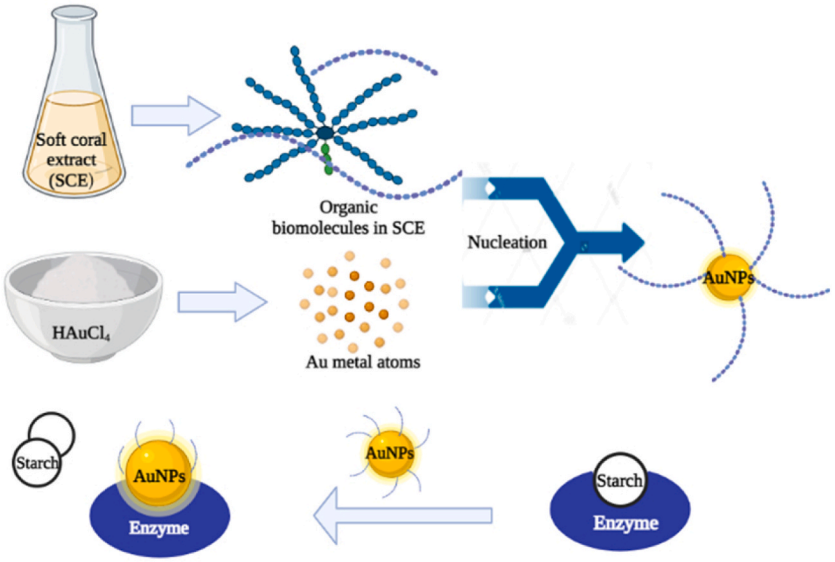

Fig. 8. Schematic diagram of synthesis of SCE-AuNPs and its α-glucosidase enzyme inhibition property.

significant. One of the possibility is that the SCE-AuNPs aggregated at higher concentrations, thereby, reducing their inhibitory function. The % inhibitions of α-glucosidase activity at variable SCE-AuNP concentrations were found to be a function of concentration-dependence. The interaction of SCE-AuNPs with these catalytic motifs in SCE-AuNPs might have changed the catalysis kinetics of α-glucosidase reactions, ultimately delaying the formation of glucose from the starch molecules. The α-glucosidase inhibitors are primarily responsible for the decline in postprandial glycemic levels and the spectrum of postprandial glucose levels. It has already been established that metal nanoparticles can inhibit α-glucosidase [31,42,51,52].

Despite enormous advancements in healthcare, the bacterial disease continues to pose a serious threat to both the aquaculture sector and public health. Novel antibacterial compounds should be developed to assist aquaculture farms and food processing units in control and management of disease and bacterial contamination in processed foods, respectively. Additionally, marine derived metabolites and their associated chemicals are thought to be a source of inventive treatment agents for a number of bacterial infections. The size, ability to attach to different molecules, and optical characteristics of the gold nanoparticles make them a strong choice for chemical and biological applications [32,53]. In current study, the antibacterial effectiveness of SCE-AuNPs against pathogenic strains of *V. cholerae* and *S. aureus* are depicted in Fig. 9a and b. The maximum inhibition zone was found in *V. cholerae* (23 ± 0.23 mm) followed by *S. aureus* (20 ± 0.15 mm) at the concentration of 100 µg/ml. Interestingly, the size of inhibition zones successively increased with response to the concentration of the SCE-AuNPs. Additionally, the bacterial cells exposed to 100 µg/ml SCE-AuNPs displayed noticeably higher levels of protein and nucleic acid leakage activity (p 0.05) than the control (Fig. 9c and d). The antibacterial efficacy of SCE-AuNPs is ascribable to the mechanisms of: (a) denaturation of bacterial cell wall and associated constituents,

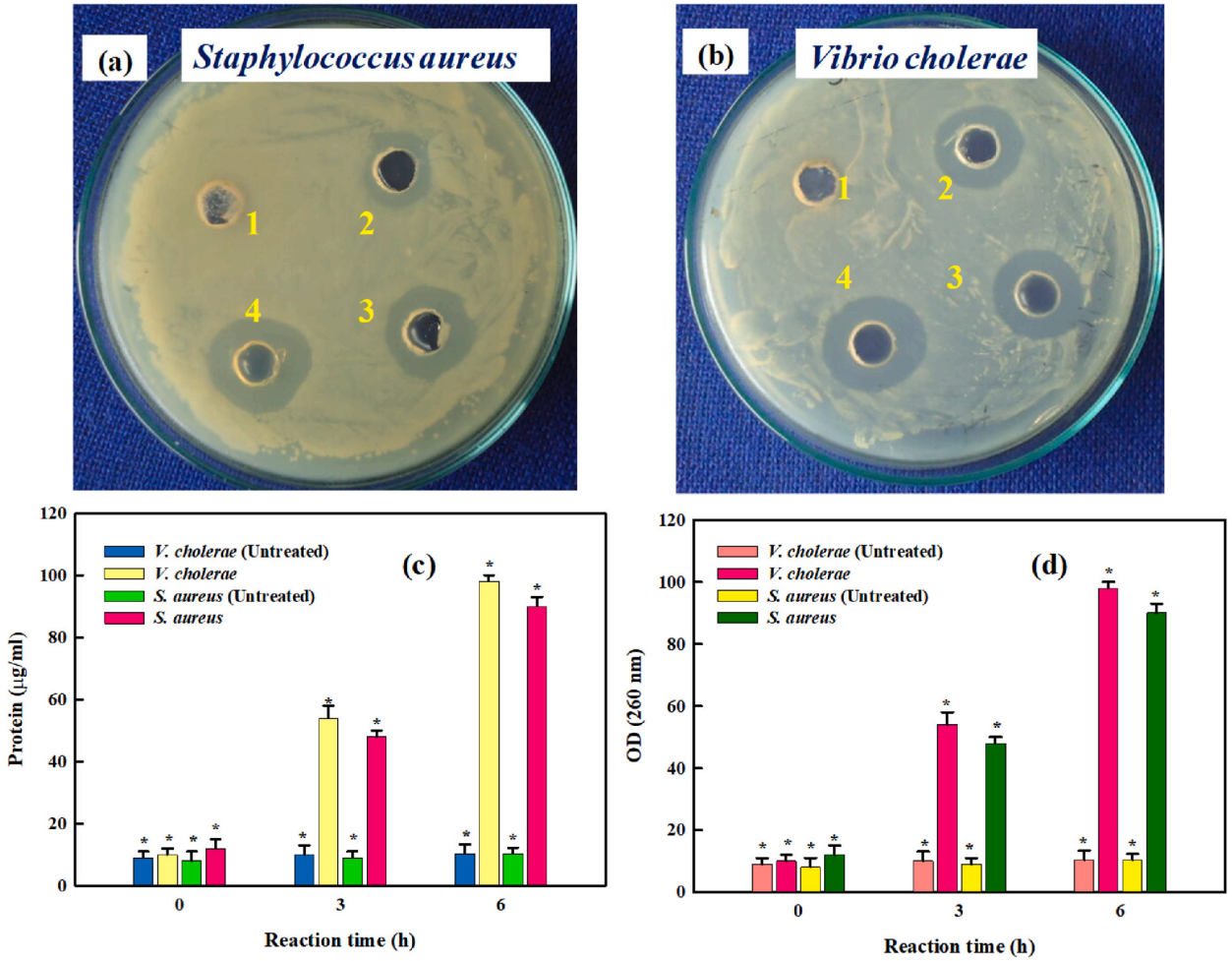

Fig. 9. Antibacterial activity of SCE-AuNPs against (a) S. aureus, (b) V. cholerae, (c) protein leakage, and (d) nucleic acid leakage. [1 = SCE; 2 = 20 µg/ml; 3 = 60 µg/ml; 4 = 100 µg/ml).

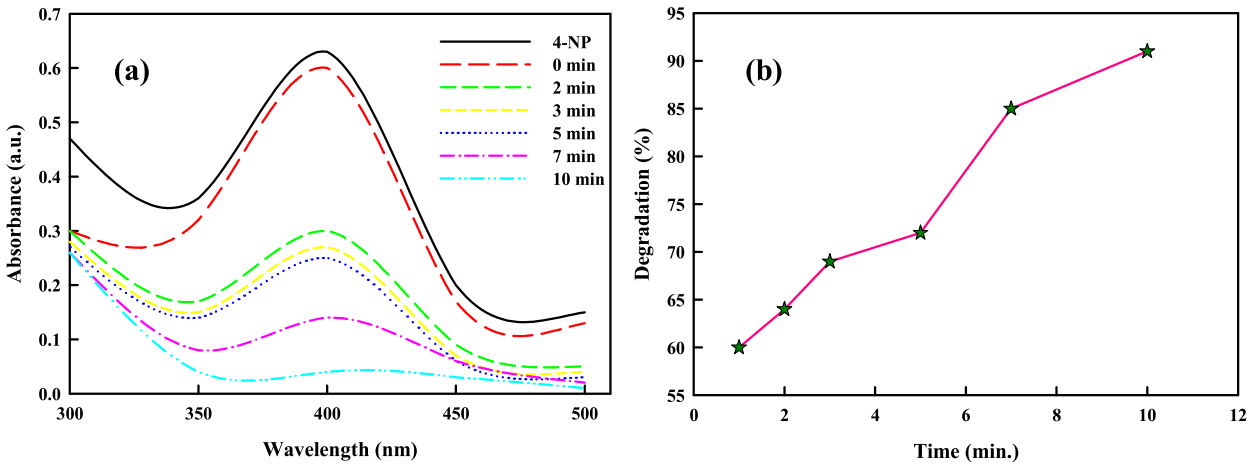

Fig. 10. (a) Ultraviolet–visible (UV–vis) spectra of 4-nitrophenol (4-NP) in presence of SCE-AuNPs, (b) Plot of percent degradation of 4-NP against time.

(b) interruption of respiratory function, (c) elimination of the outer cellular membrane, and (d) the lowering of intracellular ATP generation in infectious bacterial strains [6,7,54,55]. In the present study, the Gram-negative bacteria (*V. cholerae*) were more susceptible to SCE-AuNPs than Gram-positive cells (*S. aureus*) due to the differential cellular membranal composition between Gram-positive and Gram-negative bacteria. The Gram-negative cells have much thinner layer of cell wall as compared Gram positive ones. Furthermore, SCE-AuNPs exerted a long-lasting electrostatic attraction to the negatively charged bilayer, making it simple for the particles to permeate into the cells and cause cell death [56].

Several catalytic reactions have employed the metallic nanoparticles as catalysts. Using the reduction of MR, BPB, and 4-NP using $NaBH_4$, the catalytic potential of SCE-AuNPs has been investigated. The genotoxic and carcinogenic properties of 4-nitrophenol (4-NP) affect human, aquatic, and terrestrial environments. Additionally, due to its high stoutness and limited solubility in water, its conversion into non-toxic compounds is complicated [15]. Using a spectrophotometer, the characteristic absorption peak at 400 nm was monitored to ascertain the catalytic activity of SCE-AuNPs (200 μg/ml) in the presence of $NaBH_4$. The results showed an intriguing slow degradation of 4-NP following the addition of SCE-AuNPs to the $NaBH_4$ and 4-NP mixture. First, when $NaBH_4$ was added to 4-NP, a vivid yellowish solution was formed resulting due to the formation of sodium phenolate anions (Fig. 10a). Due to the production of nitrophenolate ion, the UV spectra at the beginning (t = 0 min) displayed a sharp band at 400 nm. Additionally, the addition of SCE-AuNPs to the reaction mixture caused a rapid decrease in absorption intensity, going from 0.60 to 0.05 in 10 min with 91% disintegration (Fig. 10b). The absorption peak at 400 nm, on the other hand, showed "status quo" for a longer period of time in the absence of SCE-AuNPs as a catalyst, indicating no decrease. The result showed that the synthetic chemical, 4-nitrophenol, is entirely degraded by SCE-AuNPs [57]. The increased rate of surfacial adsorption and larger surface area to volume ratio of SCE-AuNPs may be the rationale of the degradation of 4-NP [58,59]. First, when $NaBH_4$ was added to the reaction mixture, 4-NP was deprotonated leading to the formation of nitrophenolate ion [59]. The nitrophenolate ion was then gradually converted to 4-aminophenol (4-AP) by $NaBH_4$. The reaction and production dynamics of 4-AP were encouraged by a decline in free energy. As $NaBH_4$ was being adsorbed onto the catalyst surface, the reduction reaction commenced by the passage transfer of the BH_4 electron to the 4-NP electron acceptor phenol. As a result, the 4-NP was subsequently minimized and reduced [60]. The usage of $NaBH_4$ in the process raised the solution pH and slowed down the degradation of BH_4^- ion. This followed with a rapid oxygen depletion in the microenvironment, which led to the reduction of 4-NP. Additionally, the reaction mixture contained a good amount of the tiny bubbles surrounding the catalyst, which may have provided an encouraging environment for the reaction catalysis. Although the potential difference between acceptor and donor ($NaBH_4$) molecules slows down the reaction rate, the surplus $NaBH_4$ on hand prevents its use in oxygen reduction from altering its concentration [61].

The reduction reaction of 4-NP followed Langmuir-Hinshelwood mechanism, demonstrating the occurrence of surface adsorption via the available nanoparticle substrate on the catalyst and the surface of reducing agent [59]. It was found that ln (C_t/C_0) and time had a strong linear association, supporting the pseudo-first-order kinetics. The kinetic reaction rate constant (K) was found to be 0.122 min^{-1}, with 0.92 R^2 value calculated from the 4-NP degradation according to the plot ln (C_t/C_0) vs. time.

The colloidal solution of SCE-AuNPs was used to catalyze the reaction between BPB and MR. BPB typically exhibits absorption maxima at 590 nm. The absorbance of the BPB at 590 nm abruptly dropped from 0.30 to 0.03 with 93% degradation post addition of SCE-AuNPs (1 mg/ml) to the reaction solution of $NaBH_4$ and BPB (Fig. 11a and b). This outcome demonstrated that BPB completely degrades in the presence of $NaBH_4$ and SCE-AuNPs. Following the pseudo-first-order reaction, ln (C_t/C_0) and the passage of time exhibit a strong linear association. The BPB degradation was used to determine the kinetic reaction rate constant computed as 0.0822 min^{-1} and R^2 value as 0.91.

The dye MR exhibited absorption peak at 523 nm. Post addition of $NaBH_4$, the absorption maxima progressed to 434 nm. In addition, when the SCE-AuNPs (1 mg/ml) was added to the reaction solution of MR and $NaBH_4$, a progressive decline was observed in

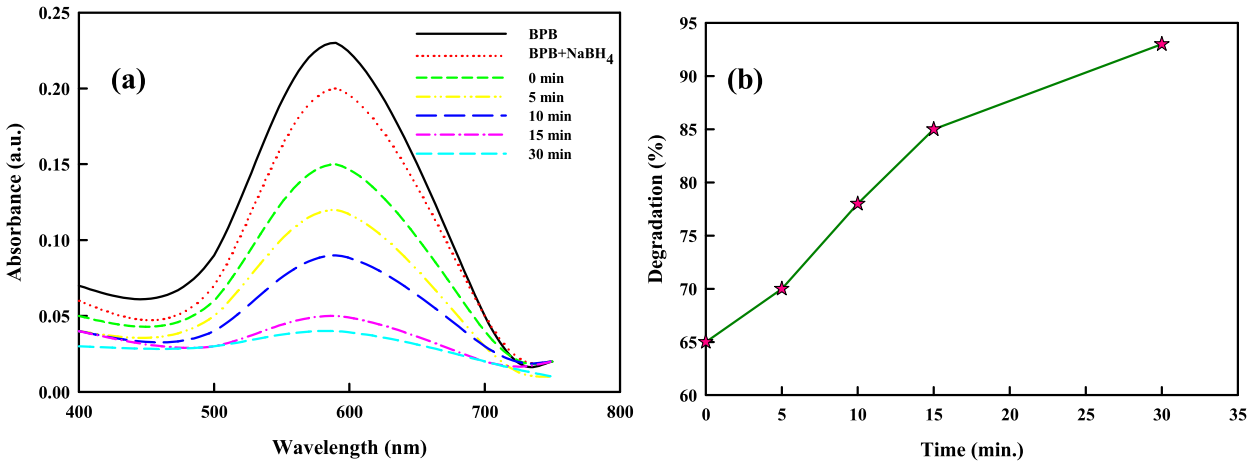

Fig. 11. (a) Ultraviolet–visible (UV–vis) spectra of bromophenol blue (BPB) in the presence of SCE-AuNPs, (b) Plot of percent degradation of BPB against time. (For interpretation of the references to colour in this figure legend, the reader is referred to the Web version of this article.)

the absorbance of MR over the course of 2 h, going from 0.07 to 0.007 with 90% degradation (Fig. 12a and b). It was discovered that ln (C_t/C_0) and time displayed a linear relationship following pseudo-first-order reaction kinetics. The reaction rate constant was found to be 0.0131 min^{-1} with 0.97 R^2 value inferred from the plot of ln (C_t/C_0) vs. time calculated from the degradation of 4-NP. It was observed that the SCE-AuNPs degraded dye MR at a slower rate in comparison to BPB and 4-NP.

The adsorption behavior of dye onto the SCE-AuNPs might be used for the elucidation and explication of the catalytic activity of SCE-AuNPs for the breakdown the pollutants produced by dye. It has been noted that $NaBH_4$ envelopes and swathes metal nanoparticles, limiting the direct contiguity of dye molecules with catalytic active site [14]. According to research, the hydride (BH_4^- and/or H^-) ion has a stronger affinity for AuNPs and forms a layer around them [62]. One of many electrochemical mechanisms, in which metal nanoparticles function as an electron relay for an oxidant and a reductant, may be used to explain the catalytic metal degradation/reduction. Further, adsorbed on the outer surface of metal particle, the BH_4^- ions donate electrons to the dye molecules via SCE-AuNPs when they are in close proximity to each other. The BH_4^- ions initially provide the electrons to SCE-AuNPs before creating a negatively charged layer around the latter [63]. Since the dye molecules have direct access to the negatively stacked SCE-AuNPs, the electrons are quickly transported to the dye molecules. Simultaneously, the passage transport of an electron lightens the color index of the pollutant and the $NaBH_4$ functions as a hydrogen supply. This hydrogen then binds with the dye molecules after an electron is transferred to the SCE-AuNPs [64,65]. Based on this, the SCE-AuNPs and BH_4^- ions react similarly, resulting in the formation of negatively charged layer all around them. This information makes a compelling case for the employment of green chemistry-based AuNP biosynthesis as an efficient catalyst for the removal of hazardous contaminants from wastewater bodies.

3. Material and methods

3.1. Chemicals

Sodium borohydride ($NaBH_4$), Chloroauric acid ($HAuCl_4.3H_2O$), potassium bromide (KBr), dyes methyl red (MR), 4-nitrophenol (4-NP), and bromophenol blue (BPB) were purchased from HiMedia.

3.2. Collection of soft coral

The specimen of marine soft coral (*Sarcophyton crassocaule*) was collected from the intertidal region of Burmanallah (11°34′22.26″N, 92°44′22.51″E), South Andaman, India in a refrigerated box and transferred to the laboratory. The sample was cleaned using autoclaved marine water to get rid of any clinging debris and related biota before being sterilized and stored. The taxonomic identification of the organism was done by using taxonomic identification keys [66,67].

3.3. Preparation of aqueous extract SCE

The method used by Ref. [32] was modified slightly to produce aqueous extract of soft coral. Using a sterile pestle and mortar, 5 g of soft coral were weighed and grounded in 50 ml of autoclaved, double-distilled water. The crude extract was thoroughly grounded before being filtered by using Whatman filter and kept in sterile storage for further use.

3.4. Biosynthesis of gold nanoparticles

50 ml 10^{-3} M $HAuCl_4.3H_2O$ solution was heated to 40–45 °C while being constantly stirred and the SCE (10 ml) was then added. The emergence of colour changes qualified the production of AuNPs formed within 30 min of the reaction. Following a thorough reduction of the solution, it was centrifuged at 10,000 g for 30 min at 4 °C. The recovered AuNPs were then redistributed in Milli-Q water.

3.5. Purification of gold nanoparticles

In order to remove unbounded phytomolecules, the biosynthesized SCE-AuNPs were washed by distilled water and subjected to centrifugation at 10,000 rpm for 15 min. The sample of pure gold nanoparticles was dried in an oven at 50 °C and used in subsequent investigations.

3.6. Characterization of biogenic gold nanoparticles

The analytical methods were used to determine the physicochemical properties of SCE-AuNPs: TEM (transmission electron microscopy); SEM (scanning electron microscopy); UV–visible spectrophotometry; zeta potential analysis; thermogravimetric analysis (TGA); and Fourier transform infrared spectroscopy (FT-IR). In addition to operating considerations, all characterization approaches, were put into practice in accordance with prior reports of [6,7].

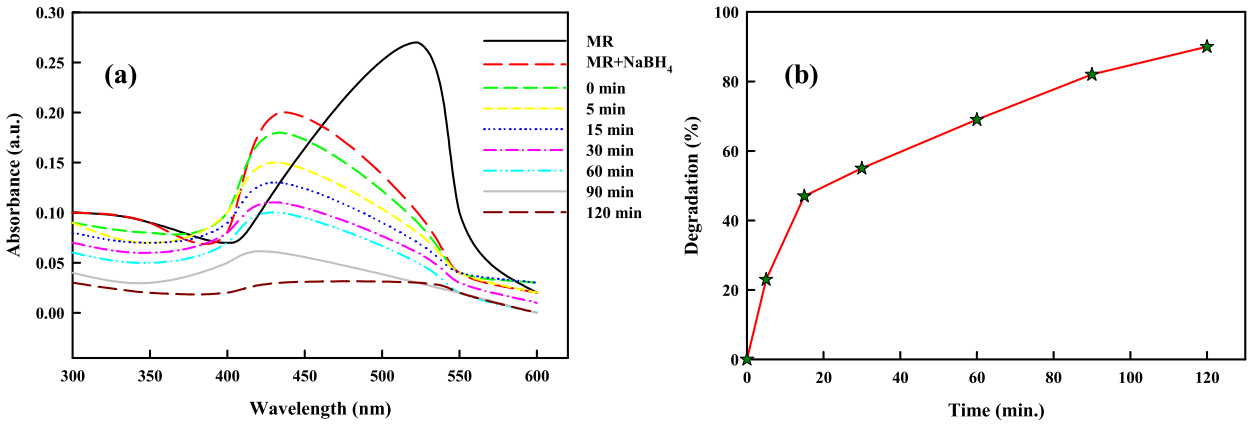

Fig. 12. (a) Ultraviolet–visible (UV–vis) spectra of methyl red (MR) in the presence of SCE-AuNPs, (b) Plot of percent degradation of MR against time. (For interpretation of the references to colour in this figure legend, the reader is referred to the Web version of this article.)

3.7. In-vitro antioxidant assays

3.7.1. DPPH radical-scavenging activity

The colour bleaching sensitivity of 2,2-diphenyl-1-picrylhydrazyl (DPPH) in methanol was used to test the electron-donating capacity (or hydrogen atom) of SCE-AuNPs [68]. A total of 50 μl of SCE-AuNPs (concentrations 20–100 μg/ml) were mixed separately with 450 μl of Tris-HCl buffer (pH = 7.4) and 1 ml of methanolic DPPH solution (0.1 mM); final volume made up to 2 ml by adding sterile distilled water and incubated at room temperature in the dark for 30 min before measuring their respective absorbance values at 517 nm. Ascorbic acid and methanol were employed as the standard and blank, respectively. The inhibitory concentration (IC50 value) at which 50% (IC50) DPPH free radical scavenging activity of SCE-AuNPs was assessed. The equation (Eq. 1) below was used to compute the percentage of DPPH radical inhibition:

$$Inhibition\ \% = \frac{([A\ Blank - B\ sample])}{A\ Blank} \times 100 \tag{1}$$

Where, A blank - the absorbance of the control reaction and B sample - is the absorbance of the test compound.

3.7.2. Reducing power assay

The reductive capability of SCE-AuNPs, i.e. the conversion of Fe^{3+} ions into Fe^{2+} ions was examined using the methods of [69,70]. The SCE-AuNPs (20–100 μg/ml; dilution with 1.0 ml double distilled water) were added with 2.5 ml of potassium ferricyanide [$K_3Fe(CN)_6$; 1%] and 2.5 ml of sodium phosphate buffer (0.2 M; pH 6.6). Prior to adding 2.5 ml of trichloroacetic acid (TCA; 10%), the sample combination was incubated at 50 °C for 20 min. The resulting mixture was centrifuged for 10 min at 3000 rpm. After combining the upper organic layer (2.5 ml) with sterile double distilled water (2.5 ml) and 0.5 ml ferric chloride ($FeCl_3$; 0.1%), the absorbance at 700 nm was measured. The percentage of reduction (Fe^{3+} to Fe^{2+} ionic state) was computed by using Eq. 1.

3.8. In-vitro anti-diabetic studies

3.8.1. α-amylase inhibitory activity

The α-amylase inhibitory activity of SCE-AuNPs was carried out using standard procedure with slight modifications [71]. In 96-well plate, 20 μl α-amylase (2 U/ml) + 20 μl SCE-AuNPs concentrations (20–100 μg/ml) were mixed with 50 μl phosphate buffer (100 mM, pH 6.9) and incubated for 20 min at 37 °C. Following then, a substrate solution of 1% soluble starch (20 μl; 100 mM phosphate buffer pH 6.9) was added and incubated for 30 min at 37 °C. Post incubation, DNS color reagent (100 μl) was added; boiled for 10 min and the absorbance was read at 540 nm. Standard (acarbose) and control mixtures were ran in parallel as control. The results were interpreted as % inhibition calculated by using equation (Eq. 2):

$$\text{Inhibition activity } (\%) = \left(1 - \frac{A}{B}\right) \times 100 \tag{2}$$

where A = absorbance of test sample and B = absorbance of control.

3.8.2. α-glucosidase inhibitory activity

All other experimental sample preparations, apart from the approach of [72], followed the instructions mentioned in section 2.7.1.

3.9. Mechanism of action of SCE-AuNPs on the microbial cells

3.9.1. Protein leakage assay

The methods of [73] were used to determine the quantification of protein constituent leakage. After being exposed to SCE-AuNPs (100 μg/ml) for 3–6 h, the bacterial cells were centrifuged (6000 rpm; 15 min). The supernatant (200 μl) and Bradford reagent (800 μl) were added to each consecutive sample before being incubated for 10 min. The optical density (at 595 nm) was measured using BSA (Bovine Serum Albumin) as a reference.

3.9.2. Nucleic acid leakage assay

The previously described standard technique of [74] with minor adjustments was used to estimate nucleic acid leakage. Aliquots of bacterial cultures were exposed to SCE-AuNPs (100 μg/ml)) for intervals of 3–6 h, post exposure were filtered through Millex-GS syringe filters (Millex-GS, Spain) with pore size of 0.2 μm; diameter 25 mm. The absorbance was measured at 260 nm.

3.10. Antibacterial activity

The antibacterial property of SCE-AuNPs was investigated by using agar well diffusion assay against Gram-positive (*Staphylococcus aureus*) and Gram-negative (*Vibrio cholerae*) bacteria [75]. In brief, the MHA medium plates were uniformly swabbed with 100 μl of pre-grown bacterial culture. Wells (10 mm in size) were made by using sterilized cork borer and the former were then subsequently filled with SCE-AuNPs (20–100 μg/ml) and incubated for 24 h at 37 °C. The formation of inhibitory zone around the wells on each plate was measured by using HiMedia antibiotic ZOI scale.

3.11. Catalytic activity and kinetic study of dye degradation by SCE-AuNPs

The catalytic activity of SCE-AuNPs was investigated by using aromatic nitro-containing compounds and dyes, MR, BPB, and 4-NP in the presence of $NaBH_4$. The reaction absorbance at 400 nm (the absorption maxima of 4-NP) was measured in relation to time by using a stock solution of 4-NP (0.4 mM) and $NaBH_4$ (40 mM). Ten milligrams of dye were added to 1 L of distilled water to make the stock solutions for MR and BPB. The dye solution was then supplemented with the appropriate amounts of SCE-AuNPs, well mixed, and the reaction progression was monitored across a range of time intervals. A control set was also kept and its absorbance was tested without the addition of nanoparticles. The degradation rate of the dye and pollutant was estimated by using Eq. (3):

$$Degradation\ rate\ (\%) = \frac{(Ao - At)}{Ao} \times 100 \tag{3}$$

where Ao is the absorbance at t = 0, At is the absorbance at time t.

The kinetics of catalytic degradation were estimated using a pseudo-first-order model, and the apparent rate constant over time was calculated using the slope of a linear correlation [76,77]. The pseudo-first-order equation (Eq. 4) was written as follows:

$$ln\frac{Ct}{Co} = -Kt \tag{4}$$

where Co is the concentration at t = 0, Ct is the concentration at time t, K is the pseudo-first-order rate constant of the degradation reaction, determined as the slope of the regression plot ln (Ct/Co) versus time (t).

3.12. Statistical analysis

Data are displayed as mean S.D. With the use of the statistical analysis programmeSigmaplot 10.1, differences between groups were ascertained using a one-way ANOVA. The p value < 0.05 was used to determine significant differences.

4. Conclusion

In present study, the first time report implying the use of aqueous extract of soft coral species, *Sarcophyton crassocaule* for the successfully biofabrication of SCE-AuNPs, which were then characterized by utilizing tools for UV, TEM, SEM, FTIR, zeta potential and TGA. Strong antioxidant activity was shown by SCE-AuNPs exhibited by DPPH and reducing power activity. Also, greenly produced SCE-AuNPs had strong α-glucosidase and α-amylase inhibitory action that was comparable to the standard medicine acarbose currently being used to treat type II diabetes.. The initial research suggests that the well-established AuNPs could be a possible therapeutic that could replace the currently used standard medication because they represent highly good environmentally acceptable materials in the field of biomedicine. Before being used, these nanoparticles also need to be warranted for their toxicity and the impact of several other biochemicals present in the environment of a living body examined in-vivo in animal systems. They exhibited strong activity against *V. cholerae* and *S. aureus* quantified by well diffusion and cellular leakage assays. Studies on the degradation of 4-NP, MR and BPB using $NaBH_4$ adhere to the pseudo-first-order paradigm, which suggests that the degradation of dye molecules by SCE-AuNPs. Hence, the SCE-AuNPs were found to be a potentially effective drug for postprandial hyperglycemia and type II diabetes, as well as the anti-bacterial and antioxidant material, and also function as a potentially effective catalyst for the decrease of anthropogenic contaminants

found in wastewater bodies.

Author contribution

Conceived and designed the experiments: Samson Rokkarukala, Tijo Cherian, Syam Mohan; **Performed the experiments**: Samson Rokkarukala Chinnasamy Ragavendran, Raju Mohanraju, C. Kamaraj; **Analyzed and interpreted the data**: Yosif Almoshari, Ahmed Albariqi, Muhammad H. Sultan, Abdullah Alsalhi; **Contributed reagents, materials, analysis tools or data:** Syam Mohan, Yosif Almoshari, Ahmed Albariqi, Muhammad H. Sultan, Abdullah Alsalhi; **Wrote the paper:** Samson Rokkarukala, Tijo Cherian, Chinnasamy Ragavendran, Raju Mohanraju, C. Kamaraj, Yosif Almoshari, Ahmed Albariqi, Muhammad H. Sultan, Abdullah Alsalhi, Syam Mohan.

Funding

This research was funded by Deputyship for Research & Innovation, Ministry of Education in Saudi Arabia through the project number ISP22-3.

Data Availability Statement

Any data related to this study can be provided upon request.

Declaration of Competing interest

The authors declare that they have no known competing financial interests or personal relationships that could have appeared to influence the work reported in this paper.

Acknowledgments

The authors extend their appreciation to the Deputyship for Research & Innovation, Ministry of Education in Saudi Arabia for funding this research work through the project number ISP22-3. The first author acknowledges Pondicherry University for providing infrastructural support. The first author acknowledges Pondicherry University for providing infrastructural support.

References

[1] H. Shabestarian, et al., Green synthesis of gold nanoparticles using *Sumac* aqueous extract and their antioxidant activity, Mat. Res. 20 (1) (2017) 264–270.
[2] T. Cherian, et al., One-pot green synthesis of biocompatible silver nanoparticles using leaf extract of *Piper nigrum*, Int. J. Pharm. Biol. Sci. (8) (2018) 1082–1088.
[3] T. Cherian, et al., Assessment of green synthetic route of silver nanoparticles synthesis by mangrove species *Rhizophora apiculata* of Andaman coast, Int. J. Pharm. Biol. Sci. 8 (2018) 819–826.
[4] T. Cherian, et al., *Myristica fragrans* bio-active ester functionalized ZnO nanoparticles exhibit antibacterial and antibiofilm activities in clinical isolates, J. Microbiol. Meth. 166 (2019), 105716.
[5] M. Camas, et al., Biosynthesis of gold nanoparticles using marine bacteria and Box–Behnken design optimization, Part. Sci. Tech. (2018), https://doi.org/10.1080/02726351.2017.1287794.
[6] T. Cherian, et al., *Cymbopogon citratus* functionalized green synthesis of CuO nanoparticles: novel prospects as antibacterial and antibiofilm agents, Biomolecules 10 (2020) 169.
[7] T. Cherian, et al., Green chemistry based gold nanoparticles synthesis using the marine bacterium *Lysinibacillus odysseyi* PBCW2 and their multitudinous activities, Nanomaterials 12 (2022) 2940.
[8] M. Ovais, et al., Biosynthesis of metal nanoparticles via microbial enzymes: a mechanistic approach, Int. J. Mol. Sci. 19 (2018) 4100.
[9] S. Mukherjee, et al., A green chemistry approach for the synthesis of gold nanoconjugates that induce the inhibition of cancer cell proliferation through induction of oxidative stress and their in vivo toxicity study, J. Mater. Chem. B. 3 (2015) 3820–3830.
[10] S. Patra, et al., Green synthesis, characterization of gold and silver nanoparticles and their potential application for cancer therapeutics, Mater. Sci. Eng. C 53 (2015) 298–309.
[11] M. Ovais, et al., Green synthesis of silver nanoparticles via plant extracts: beginning a new era in cancer theranostics, Nanomedicine 12 (2016) 3157–3177.
[12] R. Emmanuel, et al., Antimicrobial efficacy of drug blended biosynthesized colloidal gold nanoparticles from *Justicia glauca* against oral pathogens: a nanoantibiotic approach, Microb. Pathog. 113 (2017) 295–302.
[13] M. Goswami, et al., Green synthesis of silver nanoparticles supported on cellulose and their catalytic application in the scavenging of organic dyes, New J. Chem. 42 (2018) 10868–10878.
[14] P. Kumari, Abha Meena, Green synthesis of gold nanoparticles from *Lawsonia inermis* and its catalytic activities following the Langmuir-Hinshelwood mechanism, Coll. Surf. A. 606 (2020), 125447.
[15] M. Nasrollahzadeh, et al., Immobilisation of copper nanoparticles on perlite: green synthesis, characterisation and catalytic activity on aqueous reduction of 4-nitrophenol, J. Mol. Catal. Chem. 400 (2015) 22–30.
[16] T. Shah, et al., Photodegradation of bromophenol blue in aqueous medium using graphene nanoplates-supported TiO_2, Appl. Water Sci. 9 (2019) 105.
[17] W.-C. Wei, et al., Anti-inflammatory activities of natural products isolated from soft corals of Taiwan between 2008 and 2012, Mar, Drugs 11 (10) (2013) 4083–4126.
[18] J.W. Blunt, et al., Marine natural products, Nat. Prod. Rep. 28 (2011) 196–268.
[19] J.W. Blunt, et al., Marine natural products, Nat. Prod. Rep. 29 (2012) 144–222.
[20] J.W. Blunt, et al., Marine natural products, Nat. Prod. Rep. 30 (2013) 237–323.
[21] A.M. Mayer, et al., Marine pharmacology in 2007–8: marine compounds with antibacterial, anticoagulant, antifungal, anti-inflammatory, antimalarial, antiprotozoal, antituberculosis, and antiviral activities affecting the immune and nervous system, and other miscellaneous mechanisms of *action*, Comp. Biochem. Physiol. C Toxicol. Pharmacol. 153 (2011) 191–222.
[22] N. Sharma, et al., Exploitation of marine bacteria for production of gold nanoparticles, Microb. Cell Fact. 11 (2012) 86.

[23] S. Senapati, et al., Extracellular biosynthesis of bimetallic Au–Ag alloy nanoparticles, Small 1 (2005) 517–520.
[24] K. Vijayaraghavan, et al., Biosynthesis of Au(0) from Au(III) via biosorption and bioreduction using brown marine alga *Turbinaria conoides*, Chem. Engg. J. 167 (1) (2011) 223–227.
[25] A.F. Maceda, et al., Controlling the Absorption of Gold Nanoparticles via Green Synthesis Using *Sargassum crassifolium* Extract, in: Key Engineering Materials, Trans Tech Publ: Clausthal-Zellerfeld, Germany, 2018, pp. 44–48.
[26] Y. Nangia, et al., A novel bacterial isolate *Stenotrophomonas maltophilia* as living factory for synthesis of gold nanoparticles, Microb. Cell Fact. 8 (1) (2009) 2039.
[27] S. Baker, et al., Biosynthesis of gold nanoparticles by *Pseudomonas veronii* AS41G inhabiting *Annona squamosa* L, Spectrochim, Acta -A: Molecul. Biomol. Spec. 150 (2015) 691–695.
[28] M. SoltaniNejad, et al., Biosynthesis of gold nanoparticles using *Streptomyces fulvissimus* isolate, Nanomed. J. 2 (2015) 153–159.
[29] B.S. Srinath, et al., Rapid biosynthesis of gold nanoparticles by *Staphylococcus epidermidis*: its characterisation and catalytic activity, Mat. Lett. 146 (2015) 23–25.
[30] A. Annamalai, et al., Green synthesis, characterisation and antimicrobial activity of AuNPs using *Euphorbia hirta* L. leaf extract, Coll. Surf. B Biointer. 108 (2013) 60–65.
[31] M. Badeggi Umar, et al., Green synthesis of gold nanoparticles capped with procyanidins from *Leucosidea sericea* as potential antidiabetic and antioxidant agents, Biomolecules 10 (2020) 452.
[32] B. Babu, et al., Bioengineered gold nanoparticles from marine seaweed *Acanthophora spicifera* for pharmaceutical uses: antioxidant, antibacterial, and anticancer activities, Bioprocess Biosyst. Eng. 43 (2020) 2231–2242.
[33] R. Thilagam, et al., Preparation, characterisation and stability assessment of keratin and albumin functionalised gold nanoparticles for biomedical applications, Appl. Nanosci. 10 (2020) 1879–1892.
[34] A.K. Suresh, et al., Monodispersed biocompatible silver sulfide nanoparticles: facile extracellular biosynthesis using the γ-proteobacterium, *Shewanella oneidensis*, Acta Biomater. 7 (2011) 4253–4258.
[35] J.J. Antony, et al., Antimicrobial activity of *Leucas aspera* engineered silver nanoparticles against *Aeromonas hydrophila* in infected *Catla catla*, Colloid Surf. B 109 (2013) 20–24.
[36] U. Suriyakalaa, et al., Hepatocurative activity of biosynthesized silver nanoparticles fabricated reared in Xiangshan Bay, China, Aquacult, For. Rep. 3 (2013) 220–224.
[37] A.M. Elbagory, et al., Inhibition of bacteria associated with wound infection by biocompatible green synthesized gold nanoparticles from South African plant extracts, Nanomaterials 7 (2017) 417.
[38] M.M.H. Khalil, et al., Biosynthesis of Au nanoparticles using olive leaf extract: 1st Nano Updates, Arab. J. Chem. 5 (2012) 431–437.
[39] L. Falcão, et al., Tannins characterization in historic leathers by complementary analytical techniques ATR-FTIR, UV-Vis and chemical tests, J Cul.Herit. 14 (6) (2012) 499–508.
[40] M. Riaz, et al., Biogenic Synthesis of AgNPs with *Saussurea lappa* C.B. Clarke and studies on their biochemical properties, J. Nanosci. Nanotech. 18 (2018) 8392–8398.
[41] G. Sangeetha, et al., Green synthesis of zinc oxide nanoparticles by *Aloe barbadensis* miller leaf extract: structure and optical properties, Mat. Res. Bull. 46 (12) (2011) 2560–2566.
[42] K.P. Kumar, et al., Green synthesis of gold nanoparticles with *Zingiber officinale* extract: characterization and blood compatibility, Proc. Biochem. 46 (10) (2007-2013) 2011.
[43] P. Ghorbani, et al., Sumac silver novel biodegradable nano composite for bio-medical application: antibacterial activity, Molecules 20 (7) (2015) 12946–12958.
[44] M.S. Brewer, Natural antioxidants: sources, compounds, mechanisms of action, and potential applications, Compr. Rev. Food Sci. Food Saf. 10 (2011) 221–247.
[45] J. Kasthuri, et al., Biological synthesis of silver and gold nanoparticles using apiin as reducing agent, Coll. Surf. B Biointer. 68 (2009) 55–60.
[46] N. Basavegowda, et al., Phyto-synthesis of gold nanoparticles using fruit extract of *Hovenia dulcis* and their biological activities, Ind. Crops Prod. 52 (2014) 745–751.
[47] L. Du, et al., Mechanism and cellular kinetic studies of the enhancement of antioxidant activity by using surface-functionalized gold nanoparticles, Chem. Eur J. 119 (2013) 1281–1287.
[48] M.K. Swamy, et al., Synthesis and characterization of silver nanoparticles using fruit extract of *Momordica cymbalaria* and assessment of their in vitro antimicrobial, antioxidant and cytotoxicity activities, Spectrochim. Acta 151 (2015) 939–944.
[49] M.H. Oueslati, et al., Catalytic, antioxidant and anticancer activities of gold nanoparticles synthesized by kaempferol glucoside from *Lotus leguminosae*, Arab. J. Chem. 13 (2020) 3112–3122.
[50] S. Lordan, et al., The α-amylase and α-glucosidase inhibitory effects of Irish seaweed extracts, Food Chem. 141 (3) (2013) 2170–2176.
[51] P. Senthilkumar, et al., Facile green synthesis of gold nanoparticles from marine algae *Gelidiella acerosa* and evaluation of its biological potential, SN App. Sci. 1 (2019) 284.
[52] P. Senthilkumar, et al., Potent α-glucosidase inhibitory activity of green synthesized gold nanoparticles from the brown seaweed *Padina boergesenii*, Int. J. Adv. Multidiscip. Res. 2 (11) (2015 0917–0923).
[53] J. Zhang, et al., Surface chemistry of gold nanoparticles for health-related applications, Chem. Sci. 11 (2020) 923–936.
[54] E. Esquer-Miranda, et al., Effects of methanolic macroalgae extracts from *Caulerpa sertularioides* and *Ulva lactuca* on *Litopenaeus vannamei* survival in the presence of Vibrio bacteria, Fish Shellfish Immun 51 (2016) 346–350.
[55] F. Jalilian, et al., Green synthesized silver nanoparticle from *Allium ampeloprasum* aqueous extract: characterization, antioxidant activities, antibacterial and cytotoxicity effects, Adv. Powder Technol. (2020), https://doi.org/10.1016/j.apt.2020.01.011.
[56] M. Manikandakrishnan, et al., Facile green route synthesis of gold nanoparticles using *Caulerpa racemosa* for biomedical applications, J. Drug Deliv. Sci. Tec. 54 (2019), 101345.
[57] S. Khan, et al., Catalytic reduction of 4-nitrophenol and photo inhibition of *Pseudomonas aeruginosa* using gold nanoparticles as photocatalyst, J. Photochem. Photobiol. B Biol. 170 (2017) 181–187.
[58] J. Singh, et al., 'Green' synthesis of metals and their oxide nanoparticles: applications for environmental remediation, J. Nanobiotech. 16 (2018) 84.
[59] D. Ayodhya, et al., Influence of g-C_3N_4 and g-C_3N_4nanosheets supported CuS coupled system with effect of pH on the catalytic activity of 4-NP reduction using $NaBH_4$, Flat Chem 14 (2019), 100088.
[60] S.A. Aromal, et al., Characterisation and catalytic activity of gold nanoparticles synthesised using ayurvedic arishtams, Spectrochim. Acta A. Mol. Biomol. Spectrosc. 96 (2012) 1025–1030.
[61] G. Ravi, et al., Facile synthesis, characterization and enhanced catalytic reduction of 4-nitrophenol using $NaBH_4$ by undoped and Sm^{3+}, Gd^{3+}, Hf^{3+} doped La_2O_3 nanoparticles, Nano Conver 6 (2019) 12.
[62] S.M. Ansar, et al., Removal of molecular adsorbates on gold nanoparticles using sodium borohydride in water, Nano Lett. 13 (2013) 1226–1229.
[63] Z.J. Jiang, et al., Catalytic properties of silver nanoparticles supported on silica spheres, J. Phys. Chem. B 109 (2005) 1730–1735.
[64] B.K. Ghosh, et al., Preparation of Cu nanoparticle loaded SBA-15 and their excellent catalytic activity in reduction of variety of dyes, Powder Technol. 269 (2015) 371–378.
[65] X. Wang, et al., Gold nanoparticle-catalysed uranine reduction for signal amplification in fluorescent assays for melamine and aflatoxin B1, Analyst 140 (2015) 7305–7312.
[66] D.V. Rao, K. Devi, Studies of the soft coral (octocorallia: alcyonacea) of Andaman Islands, Bay of Bengal, Rec. Zoo. Sur. Ind. 206 (2003) 1–99.
[67] M.P. Janes, M.W. Lee, Octocoral Taxonomy Laboratory Manual, Results of the International Workshop on the Taxonomy of Octocorals, 2007.
[68] S.K. Lee, et al., Evaluation of the antioxidant potential of natural products, Comb. Chem. High Throughput Screen. 1 (1998) 35–46.
[69] M. Oyaizu, Studies on products of browning reaction antioxidative activities of products of browning reaction prepared from glucosamine, Jpn. J. Nutr.Diet. 44 (1986) 307–315.

[70] Q. Liu, H. Yao, Antioxidant activities of barley seeds extracts, Food Chem. 102 (2007) 732–737.
[71] A.O. Ademiluyi, G. Oboh, Aqueous extracts of roselle (*Hibiscus sabdariffa* Linn.) varieties inhibit α-amylase and α-glucosidase activities in vitro, J. Med. Food (2013) 88–93.
[72] L. Jeremia, Inhibitory effects of five medicinal plants on rat alpha-glucosidase: comparison with their effects on yeast alpha-glucosidase, J. Med. Plant Res. 5 (2014) 2863–2867.
[73] S.-H. Kim, et al., Antibacterial activity of silver-nanoparticles against *Staphylococcus aureus* and *Escherichia coli*, Microbiol. Biotechnol. Lett. 39 (2011) 77–85.
[74] A. Álvarez-Ordóñez, et al., Antibacterial activity and mode of action of a commercial citrus fruit extract, J. Appl. Microbiol. 115 (2013) 50–60.
[75] M. Vinosha, et al., Biogenic synthesis of gold nanoparticles from *Halymenia dilatata* for pharmaceutical applications: antioxidant, anti-cancer and antibacterial activities, Proc. Biochem. 85 (2019) 219–229.
[76] A. Bedoui, et al., Treatment of refractory organics contained in actual agro-industrial wastewaters by UV/H_2O_2, CLEAN – soil, air, Water 36 (2008) 373–379.
[77] N.A. Shad, et al., Synthesis of flake-like bismuth tungstate (Bi_2WO_6) for photocatalytic degradation of coomassie brilliant blue (CBB), Inorg. Chem. Commun. 86 (2017) 213–217.